King's Research Portal

Document Version
Peer reviewed version

Link to publication record in King's Research Portal

Citation for published version (APA):
Steinweg, J. K., Hui, G. T. Y., Pietsch, M., Ho, A., van Poppel, M., F A Lloyd, D., Colford, K., Simpson, J., Razavi, R., Pushparajah, K., Rutherford, M., & Hutter, J. (2021). T2* placental MRI in pregnancies complicated with fetal congenital heart disease. *Placenta*, *108*, 23-31. https://doi.org/10.1016/j.placenta.2021.02.015

Title

T2* placental MRI in pregnancies complicated with fetal congenital heart disease

Authors

Johannes K Steinweg [1]; Grace Tin Yan Hui [3]; Maximilian Pietsch[3,4], Alison Ho [3]; Milou PM van Poppel [1]; David Lloyd [1,2]; Kathleen Colford [3]; John M Simpson [1,2], Reza Razavi [1,2], Kuberan Pushparajah [1,2]; Mary Rutherford [3], Jana Hutter [3,4]

Affiliations

1. Department of Cardiovascular Imaging, School of Biomedical Engineering & Imaging Science, King's College London, London, United Kingdom
2. Department of Congenital Heart Disease, Evelina Children's Hospital, London, United Kingdom
3. Centre for the Developing Brain, King's College London, London, United Kingdom
4. Department of Biomedical Engineering, School of Biomedical Engineering & Imaging Science, King's College London, London, United Kingdom

Corresponding author

johannes.steinweg@kcl.ac.uk

Johannes K Steinweg

Department of Cardiovascular Imaging

Wellcome/EPSRC Centre for Medical Engineering

School of Biomedical Engineering & Imaging Sciences

King's College London

3rd Floor Lambeth Wing

St. Thomas' Hospital

Westminster Bridge Road

London SE1 7EH

United Kingdom

Abstract

Background

Congenital heart disease (CHD) is one of the most important and common group of congenital malformations in humans. Concurrent development and close functional links between the fetal heart and placenta emphasise the importance of understanding placental function and its influence in pregnancy outcomes. The aim of this study was to evaluate placental oxygenation by relaxometry (T2*) to assess differences in placental phenotype and function in CHD.

Methods

In this prospective cross-sectional observational study, 69 women with a fetus affected with CHD and 37 controls, whole placental T2* was acquired using a 1.5-Tesla MRI scanner. Gaussian Process Regression was used to assess differences in placental phenotype in CHD cohorts compared to our controls.

Results

Placental T2* maps demonstrated significant differences in CHD compared to controls at equivalent gestational age. Mean T2* values over the entire placental volume were lowest compared to predicted normal in right sided obstructive lesions (RSOL) (Z-Score 2.30). This cohort also showed highest lacunarity indices (Z-score -1.7), as a marker of lobule size. Distribution patterns of T2* values over the entire placental volume were positively skewed in RSOL (Z-score -4.69) and suspected, not confirmed coarctation of the aorta (CoA-) (Z-score -3.83). Deviations were also reflected in positive kurtosis in RSOL (Z-score -3.47) and CoA- (Z-score -2.86).

Conclusion

Placental structure and function appear to deviate from normal development in pregnancies with fetal CHD. Specific patterns of altered placental function assessed by T2* deliver crucial complementary information to antenatal assessments in the presence of fetal CHD.

Keywords

Introduction

Congenital heart disease (CHD) is a common group of congenital malformations with a prevalence of up to 1% of all live births, a leading cause of neonatal and infant death and a global burden in child health [1,2]. Underlying aetiology is considered multifactorial combining genetic, epigenetic and environmental causes [3–5]. Recently, placental vascular malperfusion has been reported at pathological examination in association with CHD [6,7] and it has been postulated that this may contribute to the neurodevelopmental abnormalities observed in children with CHD [8].

The placenta is the only connection between the fetal and maternal circulation. It plays a pivotal role in fetal development due to its responsibility for all fetomaternal exchange, including oxygen, carbon dioxide and nutrients, and essential immunological and homeostatic functions. The placenta and fetal heart develop concurrently and share similar developmental pathways – amplifying its unique role and vulnerability to disturbances especially in the presence of fetal CHD [9,10]. A sophisticated in vivo assessment of placental structure and function may inform understanding of complex antenatal pathophysiology in pregnancies with fetal CHD and help to identify fetuses at greater risk of adverse long term neurodevelopmental outcomes.

A common MR contrast mechanism employed to study tissue oxygen concentration is produced by the blood oxygen level dependency (BOLD) effect, exploited in quantitative T2 relaxometry (T2*). The parametric properties of deoxyhaemoglobin allow for a faster T2* decay than its oxygenated counterpart [11,12]. Widely used in functional brain MRI, it has also recently found application in placental MRI, allowing in-vivo insights into the tissue properties without the use of exogenous contrast agents [13–15].

Previous studies in humans have shown a linear negative correlation of placental mean T2* values over gestational age (GA) and found it to be predictive for low birth weight [15,16]. An increase in placental mean T2* was previously reported in response to maternal oxygen administration [17,18]. Decreased mean T2* values can be induced by vasoconstrictive agents in animal models and have been demonstrated in pregnancies with fetal growth restriction in both animals and humans [19–21]. Reduced whole placental mean T2* values for GA were recently also associated with preeclampsia [22].

Mean T2* value calculated over the placental parenchyma, either assessed in selected slices or the entire placental volume have been used for quantification in previous

93   studies. However, novel advances extend this to include spatial analysis using

94   histograms and texture-based measurements, first shown in rhesus monkeys [23,24].

95   This study aimed to evaluate whether CHD is associated with altered placental

96   phenotype and function, including signs of lower oxygenation and altered tissue

97   morphology, as estimated by high-resolution whole placental MR relaxometry (T2*) and

98   to establish methods to evaluate deviations from the expected values over GA.

Methods

In this prospective cross-sectional observational study, we recruited pregnant women carrying a fetus diagnosed with congenital heart disease (CHD) from a tertiary fetal cardiology service for CHD (St Thomas' Hospital, London, UK) alongside a control group of women with uncomplicated pregnancies during the second and third trimester. Inclusion criteria for both cohorts were singleton pregnancy, maternal age over 18 years and ability to consent in English language. Exclusion criteria for both cohorts were multiple pregnancies, major maternal health issues, any treatment for hypertension at time of scan as well as contraindications for MRI such as metallic implants and claustrophobia. Exclusion criteria for controls also included diagnosis of fetal or intrauterine growth restriction (FGR/IUGR) and low birth weight (SGA), signs of preeclampsia or (gestational) diabetes at time of scan.

Prospectively specified data collection included demographic characteristics and maternal pregnancy data at time of scan, as well as delivery notes and neonatal outcomes. Maternal data included age and BMI at scan, parity, gravida, medical history of smoking, (gestational) diabetes, hypertension, preeclampsia, HELLP syndrome, thyroid disease and anxiety or depression as noted at time of scan and in their delivery notes. Neonatal data included fetal and neonatal cardiac diagnosis, sex, GA at scan and birth, birth weight, 5 min APGAR, neonatal outcome, genetic testing, suspicion of genetic abnormality and place of birth as noted on the delivery or (cardiology) discharge notes.

Centiles and standard scores for birth weight were calculated following the INTERGROWTH-21st project [25]. SGA was defined as birthweight less than 10th centile in keeping with common clinical practice. Our CHD cohort was classified into 7 groups based on the main antenatal diagnosis (Figure 1, Table 1). We divided our cohort into left sided obstructive lesions, namely hypoplastic left heart syndrome (HLHS) and coarctation of the aorta (CoA), right-sided obstructive lesions (RSOL) defined as structural or functional obstruction of the right ventricular outflow tract, disorders of mixing (e.g., transposition of the great arteries (TGA)), suspected vascular rings (VR) and other major lesions comprising of common arterial trunk (CAT), partial anomalous pulmonary venous drainage (PAPVD) and cardiac rhabdomyomas (CR). The group of suspected CoA was further divided by those with postnatal confirmation requiring surgery within the neonatal period (CoA+) and without postnatal CoA during follow up (CoA-). All our infants are therefore followed up by our team at least until 1 year of age.

134   Ethics:

135   This study was approved by London Research Ethics Committees of the Health

136   Research Authority (HRA) of the Department of Health in the United Kingdom,

137   "Quantification of fetal brain growth and development using MRI" (REC:

138   07/H0707/105), "Fetal Imaging with Maternal Oxygen" (REC: 17/LO/0282) and "iFIND-

139   2. Further Imaging" (REC: 14/LO/1806). Controls were also included from the

140   "Placenta Imaging Project" (REC: 16/LO/1573).

141   MRI Acquisition:

142   All women were scanned using a clinical 1.5-Tesla Philips Achieva MRI with a 28-

143   channel torso coil under clinical monitoring and medical cover during the entire scan.

144   All mothers carrying a fetus with CHD were scanned in left lateral tilt. A multi-echo

145   gradient echo sequence covering the entire uterus in coronal orientation was acquired

146   with a resolution of 2.5mm isotropic, FOV=360x360, 50-88 slices, no SENSE, no half-

147   scan, TR=14s, TE=11.376ms / 57.313ms / 103.249ms / 149.186ms / 195.122ms, free

148   breathing, TA=1min.

149   MRI data processing:

150   T2* maps were calculated using an in-house monoexponential fitting in MATLAB (The

151   MathWorks Inc, USA). The whole placenta was manually segmented by experienced

152   observers (JKS, GH, AH, JH) using ITK-SNAP [26], with exactly matched instructions

153   to segment the placenta conservatively, avoiding inclusion of both amniotic fluid and

154   maternal vasculature. Reproducibility of manual segmentations between observers

155   was assessed using the Sørensen–Dice coefficient [27].

156   The masks were automatically refined by excluding non-physiological values. Mean

157   T2*, skewness, kurtosis and lacunarity values were obtained using a purpose-build

158   python script [13,28]. Lacunarity values thereby reflect the spatial distribution of gaps of

159   a specific size within lobules [29] and a box-size matched to typical placental lobule

160   size.

161   To estimate placental development over GA we used Gaussian Process Regression

162   (GPR), a Bayesian non-parametric regression [30]. Clinical cohorts are inherently

163   heterogenous necessitating an estimation of uncertainty of probable distributions.

164   Accounting for this and a covariance between the data points GPR provides normative

165   group mean function, allowing point estimates and predictive confidence for each

166   observation. This allows the calculation of standard (Z-) scores for all measured test

167   data points, describing the distance to expected value following the normative group

168   mean function [31].

169   The control cohort was split into training and test data (0.7 to 0.3 ratio) and the test
170   subjects were used to train the model. The kernel function used was an additive
171   combination of Constant function, Radial Basis Functions and Noise kernel. The data
172   was scaled pre-training. Predictive posterior distributions were obtained for mean T2*,
173   lacunarity, skewness and kurtosis separately. Z-scores for the observed values were
174   derived for all CHD cohorts by estimation of mean deviation and median deviation from
175   GPR predicted value normalised by the prediction uncertainty.
176   For comparison of clinical parameters controls were restricted to GA at scan between
177   28 and 37 weeks to match GA for CHD cohort, categorical variables were compared
178   using Fisher's exact test, continuous variables were evaluated for normality by Shapiro
179   compared using Independent T-test (normal distribution), 2-tailed Mann-Whitney U test
180   (non-normal distribution). Dependence of results from clinical parameters was
181   evaluated by coefficient of determination. All statistical analysis and visualisation were
182   performed using SPSS Statistics v27 (IBM) and Jupyter Notebook, python3.

183

Results

Maternal and neonatal demographics are demonstrated in Table 1. Overall, 119 participants were enrolled in this study. Eight subjects from our CHD cohort were excluded: for twin pregnancy (n=1), insufficient scan data (n=3) and insufficient outcome data at time of analysis (n=4). Five controls were excluded for small for GA at birth (n=3) and insufficient scan data (n=2). In total 69 women with pregnancies with fetal diagnosis of CHD and 37 women with uncomplicated pregnancies were included in the analysis (Figure 1). The median GA at scan was 31.3 weeks (IQR 2.21) and 31.2 weeks (IQR 8.11) respectively. Results of genetic testing from antenatal invasive procedures or postnatal blood sample using at least array comparative genomic hybridization (aCGH) were available for 46 (67%) subjects in our CHD cohort. 5/46 identified an abnormal result (two with Chr 2q31 deletion, one with a Chr 9 deletion and gene copy number on Chr 2, one with TSC1 gene mutation, and one with mosaic Monosomy X). All remaining patients caused no phenotypic suspicion for a genetic abnormality after birth.

Seven newborns with CHD from our cohort died due to necrotising enterocolitis (1), hypoxic ischemic encephalopathy (1), congenital diaphragmatic hernia (1) and cardiac collapse or palliation (4). The CHD cohort had a higher incidence of low APGAR score (<7) at 5 minutes (p=0.024) compared to our control cohort. GA at birth (p<0.001) and birth weight (p<0.001) and birth head circumference (p=0.005) were significantly lower in the CHD cohort, whose mothers were also younger (p=0.017). None of the other clinical collected parameters achieved clinical significance.

We have reviewed medical records at time of scan and delivery. Our CHD cohort included three women diagnosed with preeclampsia (4.3%). Two needed delivery at 32 weeks of gestation, one for severe HELLP and one for uncontrollable hypertension. One woman delivered after induction early term at 37 weeks of GA.

In our CHD cohort 18 (26%) newborns were born <10th birth weight centile (SGA), 25 (36%) newborns were born with low head circumference (HC) <10th centile, 13 newborns (19%) were SGA and had low HC. Only one of these 13, would be defined as growth restricted following the consensus-based definition in the newborn by Beune et al. [32].

Placental histology was available in 12 pregnancies complicated by fetal CHD on special clinical request mostly due to maternal pyrexia during delivery (Supplemental Table 1). From the two placentas demonstrating signs of maternal vascular malperfusion (MVM), one placenta showed also acute subchorionitis and maternal

219 inflammatory response (MIR) in keeping with ascending intra-uterine infection showing
220 infarcts of variable age, but no thrombi. The other placenta was from a patient
221 diagnosed with severe preeclampsia and HELLP syndrome leading to early delivery.
222 Placental histology was also available for 15 control subjects as part of other study
223 protocols (Supplemental Table 1).

Qualitative assessments

225 Placental T2* maps in our cohort of RSOL showed most marked differences compared
226 to age-matched controls as depicted in mid-parenchymal slices (Figure 2). Specifically,
227 short T2* values were noted in the entire placenta with additional and faster decay from
228 the centre to the periphery of the lobules. Furthermore, increased heterogeneity could
229 be observed in RSOL. Our cohorts of left sided obstructive lesions, disorders of mixing
230 and other lesions appeared only moderately different to controls at similar GA (Figure
231 2). Overall, our CHD cohort appeared to have generally lower signal intensity
232 throughout the placenta, advanced lobularity and higher granularity within the lobules
233 at a given GA compared to our control cohort.

Quantitative assessments

235 Interobserver variability of manually segmented placental masks showed good
236 correlation in 10 randomly selected with a Sørensen–Dice coefficient of 0.87.
237 Quantitative results from the control cohort illustrate decay in mean T2* with increasing
238 GA, in keeping with previous literature [15,29]. Lacunarity, kurtosis and skewness tend
239 to increase over GA in all our cohorts as previously shown in controls [28]. The
240 obtained posterior mean of the Gaussian process is given for all quantitative values in
241 Figure 3.
242 Mean T2* values over the entire placental volume were lowest compared to predicted
243 normal in RSOL (Z-Score 2.30) and our cohort with other major lesions [CAT, PAPVD,
244 CR] (Z-Score 2.31). Our CoA- cohort had a larger deviation from expected values (Z-
245 Score 1.39) than CoA+ (Z-score 0.24). Mean T2* values for HLHS (Z-score 0.63), VR
246 (0.09) and TGA (Z-score -0.11) were within one standard deviation (SD) from expected
247 results.
248 RSOL (Z-score -1.7), our group of other major lesions (Z-score -1.26) and CoA- (Z-
249 score -1.02) showed significantly higher lacunarity compared to expected results at GA
250 equivalent. HLHS (Z-score -0.18), TGA (Z-score -0.01) and suspected VR (Z-score
251 0.06) were similar to expected controls. CoA+ showed slightly lower lacunarity (Z-score
252 0.26).

253 Distribution of T2* values over the entire placental volume was positively skewed in

254 RSOL (Z-score -4.69) and CoA- (Z-score -3.83), followed by our group of other major

255 lesions (Z-score -1.75) and HLHS (Z-score -1.12). Suspected VR (Z-score -0.8), CoA+

256 (Z-score -0.66) distributions were positively skewed within one SD. Our TGA cohort

257 was closest to expected skewness (Z-score 0.02).

258 We found positive kurtosis of distribution most significantly in RSOL with highest mean

259 deviation (Z-score -3.47), followed by CoA- (Z-score -2.86) and our group of other

260 major lesions (Z-score -1.97). HLHS and CoA+ showed positive kurtosis with almost

261 one SD from expected results (Z-Scores -0.98), while suspected VR (Z-score -0.73)

262 and TGA (Z-Score -0.27) showed similar kurtosis of distribution compared to our

263 control cohort.

264 All placentas (19/69, 28%) with individual z-scores $> \pm 3$ for any of calculated results

265 were individually reviewed for correlation with clinical confounders, while we found

266 MVM in two placentas and SGA complicating one pregnancy, overall numbers did not

267 reach statistical significance.

268 Mean and median deviation form GP (Z-score) for all cohorts and measured values are

269 listed in Table 2. Individual heterogeneity is demonstrated in histograms of occurrence

270 fraction of T2* values in all voxels within the individual placenta from all participants in

271 Figure 4. These histograms are color-coded by results of genetic testing in

272 Supplemental Figure 1.

273 Maternal BMI at scan did not have an effect on mean T2* values (R^2 = 0.004). Maternal

274 lie supine or left lateral, 30 and 7 scans respectively, had no significant effect on mean

275 T2* values in our control group (p = 0.44). Placental position dichotomised in mostly

276 anterior or posterior was also not associated with mean T2* values (p = 0.98). There

277 was no linear correlation with mean T2* Z-scores at scan and weight (R^2 = 0.13) or

278 head circumference at birth (R^2 = 0.11).

Discussion

In this study we have shown for the first time a comprehensive approach to placental tissue characterisation in CHD. Using T2 relaxometry (T2*) and Gaussian Process Regression (GPR) we were able to provide standard deviations for a range of placental metrics across various CHD groups from predicted values derived by our model trained on a control group. Mean T2* values over the entire placenta may not represent regional differences adequately and can lead to misinterpretation of imaging findings. Therefore, we also used histograms and evaluated skewness and kurtosis to show specific pattern of distribution depending on CHD subtype, which in turn may represent pathophysiological substrates.

Requiring minimal acquisition time (<1min) and minor modification to clinical scan protocols, these baseline placental assessments have been included into all our clinical fetal MRI scans.

While mean T2* deviation for RSOL (Z-score 2.30) is comparable with our group of other cardiovascular lesions (Z-score 2.31), the latter shows much less deviation from calculated normal distribution as described in skewness and kurtosis (Z-scores -1.75 and -1.97, respectively). Strikingly, right-sided obstructive lesions (RSOL) show highest deviation from expected normal distribution represented in skewness (Z-score -4.69) and kurtosis (Z-score -3.47).

Our findings of abnormal placental imaging appear CHD lesions specific. One might speculate that common intrinsic developmental pathways of placenta and fetal heart may play a larger role, warranting further investigations towards understanding the pathophysiology. Future investigations in conjunction with assessments of fetal circulation in the presence of CHD, a flourishing field in both ultrasound and MRI research [33,34], may allow a more detailed interpretation of our results.

Given the severe implications after birth, the cohort of HLHS appears to have surprisingly limited deviations from control in placental structure and function. This suggests less co-dependence between the development and or antenatal effects of this anomaly and the development and function of the placenta also requiring further research.

Our findings are in keeping with data from a very large Danish cohort from Matthiesen et al. also depicting an association of RSOL, but not left outflow tract obstructions including HLHS, aortic valve stenosis, and coarctation of the aorta, with lower placental weight [35]. Moreover Llurba et al. have suggested an imbalance in maternal and fetal

313   angiogenic factors may contribute to CHD and placental dysfunction most marked in

314   cohorts other than left sided lesions [36].

315   Fetuses with antenatal suspicion of CoA without confirmation after birth (CoA-) were

316   purposely not classified as controls in the design of this study. Firstly, presentation of

317   CoA may present several weeks (up to a year) after closure of the arterial duct [37].

318   None of the infants included here showed signs of coarctation at the time of manuscript

319   preparation. Secondly, there is a growing evidence that the observed ventricular

320   asymmetry is a feature of abnormal loading conditions leading to abnormal myocardial

321   deformation in fetuses with suspected coarctation [38]. In turn our CoA cohort spreads

322   relatively widely through the range of values provided by our placental assessments

323   (Supplemental Figure 2), which may reflect the wide clinical spectrum of CoA+

324   observed after birth, but also may indicate previously underexplored CHD entities

325   some of which do not require an extensive surgical arch repair within the first year of

326   life.

327   Studies of placental dysfunction and vascular malperfusion have shown altered

328   baseline conditions on assessment with T2 relaxometry accounting for a higher relative

329   response to maternal hyperoxygenation [15]. In our study we show similar altered

330   placental baseline conditions in case of fetal CHD. This is a critical insight to

331   understand the reported effects of short term maternal hyperoxygenation in CHD,

332   which are being explored to improve fetal oxygenation in CHD [39].

333   Altered placental baseline functions are of particular importance to understand the

334   complex intertwined fetomaternal environment in CHD and will also be essential to

335   understand further approaches on antenatal intervention such as maternal

336   hyperoxygenation [40].

337   Furthermore, structural assessments based on T2-weighted, and more recently also T1

338   imaging, depict changes over GA encompassing advanced lobulation with varied

339   lobule sizes, higher granularity, and substantial areas of low-signal intensity and an

340   increasing microstructural heterogeneity [41]. These changes are pronounced in FGR

341   or PE compared to healthy controls [22,42]. Although we did not report weighted MR

342   imaging in this study, observations from our T2* maps of increasing lacunarity over GA

343   is in keeping with the literature for our control and CHD cohort. Moreover, our CHD

344   cohorts also present higher lacunarity compared to healthy controls, most pronounced

345   in RSOL (Z-score -1.70).

346   As previously reported factors such as maternal age, BMI, fetal sex, parity, mode of

347   delivery and placental location were not correlated with T2* once corrected for GA [28].

Limitations of this study

Although we are based at a major referral centre for congenital heart disease in the UK, this was a single centre study, with some patients delivering outside of our hospital, having been referred for antenatal imaging. Our CHD groups are of moderate sample size and may influence statistical significance.

Our placental scan protocol consistent of one single timepoint, therefore temporal variance in placental T2* measurements, as recently suggested by other groups, might not be accounted for in our data [43]. Recent literature describes also the possible influence of maternal or placental position on T2* signals in higher field MRI [44]. While we have scanned all our CHD patients in left lateral position, controls were also scanned supine, resulting in higher statistical variance, 371.6 vs 776.5 respectively, but not reaching statistical significance.

While in-utero MRI provides an excellent opportunity to provide early, in-vivo evidence for specific placental phenotypes associated with CHD and hence a window of observation into the intertwined relation between developing heart and placenta, it cannot directly answer the question on causality and order of events.

Despite recent attempts to standardize definitions for FGR/IUGR, there is currently no universal definition, which would include fetuses with congenital malformations such as CHD [45]. Furthermore, the recent consensus-based definition of growth restriction on the newborn excludes congenital and chromosomal abnormalities specifically, although stating it may be applicable for this group due to the lack of any other option [32]. Previous literature, including a large population of 924,422 cohorts with over 5500 CHD cases from Denmark also suggests an association of some CHD subtypes with lower birth weight and head circumference [46]. Therefore, we did not exclude any participants in our CHD cohort solely due diagnosis for FGR/IUGR or SGA.

Placental histopathology results were only available in 25% of all our assessments and in CHD patients only with a specific clinical question at time of birth, such as maternal pyrexia. Statistical analysis of features of MVM or fetal vascular malperfusion (FVM) or Chorioamnionitis could therefore not be included. Similarly, only two placentas showed infarcts in histopathology. These could be identified on the in-vivo imaging but did not significantly alter the observed whole placental mean T2* results and have therefore not been factored in the statistical analysis. Previous literature from postnatal placental histopathology describe increased findings of FVM and MVM in the presence of preeclampsia as well as CHD supporting the hypothesis of similar etiopathogenetic factors contributing to the development of placental malformation and CHD [6].

383   While T2* values are an indicator of oxygen concentration, direct measurement was

384   not possible in our setting. Oxygen-haemoglobin dissociation curves derived from MRI

385   in animal models might be available for future studies to allow close estimation of

386   actual oxygen content in the fetoplacental circulation [47,48].

387   Including only five pregnancies with confirmed fetal chromosomal abnormalities in our

388   cohort did not allow for further statistical analysis of potential associations. This study

389   did not include volumetric assessments of the placenta given echo planar imaging is

390   associated with geometric distortions.

391   Future studies applied to CHD cohorts with more complex and time-consuming scan

392   protocols, including diffusion-weighted imaging or texture analysis using T1 and T2

393   weighted methods, may allow modelling of fetal and maternal peculiarities in circulation

394   and disentangle tissue characteristics and flow pathophysiology, as recently in CHD

395   cohorts [41,49–51]. Slator et al. have recently published a study with a focused

396   extensive research protocol on the microenvironments within the placenta depicting

397   heterogenous compartments from maternal and fetal side [52]. Using Velocity-

398   Selective Arterial Spin Labelled MRI Zun et al. also reported that global placental

399   perfusion significantly decreased and regional variation of placental perfusion

400   significantly increased over GA in fetuses with CHD [53,54].

401

Conclusion

403   This study describes in vivo differences in placental tissue phenotypes in healthy

404   controls and fetuses with antenatal diagnosis of congenital heart disease based on T2

405   relaxometry. Using machine learning we depict unique features of T2* value

406   distribution and their standard score from our normal cohort for a wide range of major

407   cardiac lesions, providing information on placental dysfunction complementary in the

408   antenatal assessment of CHD.

Acknowledgements

Funding

Declaration of competing interests

The authors declare that they have no competing interest.

Keywords

References

[1] T. van der Bom, A.C. Zomer, A.H. Zwinderman, F.J. Meijboom, B.J. Bouma, B.J.M. Mulder, The changing epidemiology of congenital heart disease, Nature Reviews Cardiology. 8 (2011) 50–60. https://doi.org/10.1038/nrcardio.2010.166.

[2] M.S. Zimmerman, A.G.C. Smith, C.A. Sable, M.M. Echko, L.B. Wilner, H.E. Olsen, H.T. Atalay, A. Awasthi, Z.A. Bhutta, J.L. Boucher, F. Castro, P.A. Cortesi, M. Dubey, F. Fischer, S. Hamidi, S.I. Hay, C.L. Hoang, C. Hugo-Hamman, K.J. Jenkins, A. Kar, I.A. Khalil, R.K. Kumar, G.F. Kwan, D.T. Mengistu, A.H. Mokdad, M. Naghavi, L. Negesa, I. Negoi, R.I. Negoi, C.T. Nguyen, H.L.T. Nguyen, L.H. Nguyen, S.H. Nguyen, T.H. Nguyen, M.R. Nixon, J.J. Noubiap, S. Patel, E.K. Peprah, R.C. Reiner, G.A. Roth, M.-H. Temsah, M.R. Tovani-Palone, J.A. Towbin, B.X. Tran, T.T. Tran, N.T. Truong, T. Vos, K. Vosoughi, R.G. Weintraub, K.G. Weldegwergs, Z. Zaidi, B. Zheleva, L. Zuhlke, C.J.L. Murray, G.R. Martin, N.J. Kassebaum, Global, regional, and national burden of congenital heart disease, 1990–2017: a systematic analysis for the Global Burden of Disease Study 2017, The Lancet Child & Adolescent Health. 4 (2020) 185–200. https://doi.org/10.1016/S2352-4642(19)30402-X.

[3] D.K. Jarrell, M.L. Lennon, J.G. Jacot, Epigenetics and Mechanobiology in Heart Development and Congenital Heart Disease, Diseases. 7 (2019) 52. https://doi.org/10.3390/diseases7030052.

[4] Russell Mark W., Chung Wendy K., Kaltman Jonathan R., Miller Thomas A., Advances in the Understanding of the Genetic Determinants of Congenital Heart Disease and Their Impact on Clinical Outcomes, Journal of the American Heart Association. 7 (2018) e006906. https://doi.org/10.1161/JAHA.117.006906.

[5] S. Zaidi, M. Choi, H. Wakimoto, L. Ma, J. Jiang, J.D. Overton, A. Romano-Adesman, R.D. Bjornson, R.E. Breitbart, K.K. Brown, N.J. Carriero, Y.H. Cheung, J. Deanfield, S. DePalma, K.A. Fakhro, J. Glessner, H. Hakonarson, M.J. Italia, J.R. Kaltman, J. Kaski, R. Kim, J.K. Kline, T. Lee, J. Leipzig, A. Lopez, S.M. Mane, L.E. Mitchell, J.W. Newburger, M. Parfenov, I. Pe'er, G. Porter, A.E. Roberts, R. Sachidanandam, S.J. Sanders, H.S. Seiden, M.W. State, S. Subramanian, I.R. Tikhonova, W. Wang, D. Warburton, P.S. White, I.A. Williams, H. Zhao, J.G. Seidman, M. Brueckner, W.K. Chung, B.D. Gelb, E. Goldmuntz, C.E. Seidman, R.P. Lifton, De novo mutations in histone-modifying genes in congenital heart disease, Nature. 498 (2013) 220–223. https://doi.org/10.1038/nature12141.

462 [6] H. Miremberg, L. Gindes, L. Schreiber, A.R. Sternfeld, J. Bar, M. Kovo, The
463   association between severe fetal congenital heart defects and placental vascular
464   malperfusion lesions, Prenatal Diagnosis. 39 (2019) 962–967.
465   https://doi.org/10.1002/pd.5515.
466 [7] J. Binder, S. Carta, J.S. Carvalho, E. Kalafat, A. Khalil, B. Thilaganathan, Evidence
467   for uteroplacental malperfusion in fetuses with major congenital heart defects,
468   PLOS ONE. 15 (2020) e0226741. https://doi.org/10.1371/journal.pone.0226741.
469 [8] S.D. Schlatterer, J. Murnick, M. Jacobs, L. White, M.T. Donofrio, C. Limperopoulos,
470   Placental Pathology and Neuroimaging Correlates in Neonates with Congenital
471   Heart Disease, Sci Rep. 9 (2019). https://doi.org/10.1038/s41598-019-40894-y.
472 [9] G.J. Burton, E. Jauniaux, Development of the Human Placenta and Fetal Heart:
473   Synergic or Independent?, Front. Physiol. 9 (2018).
474   https://doi.org/10.3389/fphys.2018.00373.
475 [10] J.A. Courtney, J.F. Cnota, H.N. Jones, The Role of Abnormal Placentation in
476   Congenital Heart Disease; Cause, Correlate, or Consequence?, Frontiers in
477   Physiology. 9 (2018) 1045. https://doi.org/10.3389/fphys.2018.01045.
478 [11] L. Pauling, C.D. Coryell, The Magnetic Properties and Structure of Hemoglobin,
479   Oxyhemoglobin and Carbonmonoxyhemoglobin, Proceedings of the National
480   Academy of Sciences. 22 (1936) 210–216. https://doi.org/10.1073/pnas.22.4.210.
481 [12] S. Ogawa, T.-M. Lee, A.S. Nayak, P. Glynn, Oxygenation-sensitive contrast in
482   magnetic resonance image of rodent brain at high magnetic fields, Magnetic
483   Resonance in Medicine. 14 (1990) 68–78.
484   https://doi.org/10.1002/mrm.1910140108.
485 [13] J. Hutter, P.J. Slator, L. Jackson, A.D.S. Gomes, A. Ho, L. Story, J.
486   O'Muircheartaigh, R.P.A.G. Teixeira, L.C. Chappell, D.C. Alexander, M.A.
487   Rutherford, J. V. Hajnal, Multi-modal functional MRI to explore placental function
488   over gestation., Magnetic Resonance in Medicine. 81 (2019) 1191–1204.
489   https://doi.org/10.1002/mrm.27447.
490 [14] M.C. Schabel, V.H.J. Roberts, J.O. Lo, S. Platt, K.A. Grant, A.E. Frias, C.D.
491   Kroenke, Functional imaging of the nonhuman primate Placenta with endogenous
492   blood oxygen level–dependent contrast, Magnetic Resonance in Medicine. 76
493   (2016) 1551–1562. https://doi.org/10.1002/mrm.26052.
494 [15] M. Sinding, D.A. Peters, S.S. Poulsen, J.B. Frøkjær, O.B. Christiansen, A.
495   Petersen, N. Uldbjerg, A. Sørensen, Placental baseline conditions modulate the

496   hyperoxic BOLD-MRI response., Placenta. 61 (2018) 17–23.

497   https://doi.org/10.1016/j.placenta.2017.11.002.

498 [16]C. Wright, D.M. Morris, P.N. Baker, I.P. Crocker, P.A. Gowland, G.J. Parker, C.P.

499   Sibley, Magnetic resonance imaging relaxation time measurements of the

500   placenta at 1.5T, Placenta. 32 (2011) 1010–1015.

501   https://doi.org/10.1016/j.placenta.2011.07.008.

502 [17]I. Huen, D.M. Morris, C. Wright, G.J.M. Parker, C.P. Sibley, E.D. Johnstone, J.H.

503   Naish, R 1 and R 2 * changes in the human placenta in response to maternal

504   oxygen challenge, Magnetic Resonance in Medicine. 70 (2013) 1427–1433.

505   https://doi.org/10.1002/mrm.24581.

506 [18]A. Sørensen, D. Peters, C. Simonsen, M. Pedersen, B. Stausbøl-Grøn, O.B.

507   Christiansen, G. Lingman, N. Uldbjerg, Changes in human fetal oxygenation

508   during maternal hyperoxia as estimated by BOLD MRI., Prenatal Diagnosis. 33

509   (2013) 141–5. https://doi.org/10.1002/pd.4025.

510 [19]E. Ingram, D. Morris, J. Naish, J. Myers, E. Johnstone, MR imaging measurements

511   of altered placental oxygenation in pregnancies complicated by fetal growth

512   restriction, Radiology. 285 (2017) 953–960.

513   https://doi.org/10.1148/radiol.2017162385.

514 [20]G.E. Chalouhi, M. Alison, B. Deloison, R. Thiam, G. Autret, D. Balvay, C.A.

515   Cuenod, O. Clément, L.J. Salomon, N. Siauve, Fetoplacental Oxygenation in an

516   Intrauterine Growth Restriction Rat Model by Using Blood Oxygen Level–

517   Dependent MR Imaging at 4.7 T, Radiology. 269 (2013) 122–129.

518   https://doi.org/10.1148/radiol.13121742.

519 [21]E. Girsh, V. Plaks, A.A. Gilad, N. Nevo, E. Schechtman, M. Neeman, N. Dekel,

520   Cloprostenol, a Prostaglandin F(2alpha) Analog, Induces Hypoxia in Rat

521   Placenta: BOLD Contrast MRI, NMR in Biomedicine. 20 (2007) 304–325.

522   https://doi.org/10.1002/nbm.

523 [22]A.E.P. Ho, J. Hutter, L.H. Jackson, P.T. Seed, L. Mccabe, M. Al-adnani, A.

524   Marnerides, S. George, L. Story, J. V Hajnal, M.A. Rutherford, L.C. Chappell, T2 *

525   Placental Magnetic Resonance Imaging An Observational Cohort Study,

526   Hypertension (Dallas, Tex. : 1979). (2020) 1–9.

527   https://doi.org/10.1161/HYPERTENSIONAHA.120.14701.

528 [23]A.J. Hirsch, V.H.J. Roberts, P.L. Grigsby, N. Haese, M.C. Schabel, X. Wang, J.O.

529   Lo, Z. Liu, C.D. Kroenke, J.L. Smith, M. Kelleher, R. Broeckel, C.N. Kreklywich,

530   C.J. Parkins, M. Denton, P. Smith, V. DeFilippis, W. Messer, J.A. Nelson, J.D.

531   Hennebold, M. Grafe, L. Colgin, A. Lewis, R. Ducore, T. Swanson, A.W. Legasse,

532   M.K. Axthelm, R. MacAllister, A.V. Moses, T.K. Morgan, A.E. Frias, D.N.

533   Streblow, Zika virus infection in pregnant rhesus macaques causes placental

534   dysfunction and immunopathology, Nature Communications. 9 (2018) 263.

535   https://doi.org/10.1038/s41467-017-02499-9.

536   [24]J.O. Lo, V.H.J. Roberts, M.C. Schabel, X. Wang, T.K. Morgan, Z. Liu, C.

537   Studholme, C.D. Kroenke, A.E. Frias, Novel Detection of Placental Insufficiency

538   by Magnetic Resonance Imaging in the Nonhuman Primate:, Reproductive

539   Sciences. (2017). https://doi.org/10.1177/1933719117699704.

540   [25]J. Villar, L. Cheikh Ismail, C.G. Victora, E.O. Ohuma, E. Bertino, D.G. Altman, A.

541   Lambert, A.T. Papageorghiou, M. Carvalho, Y.A. Jaffer, M.G. Gravett, M. Purwar,

542   I.O. Frederick, A.J. Noble, R. Pang, F.C. Barros, C. Chumlea, Z.A. Bhutta, S.H.

543   Kennedy, International Fetal and Newborn Growth Consortium for the 21st

544   Century (INTERGROWTH-21st), International standards for newborn weight,

545   length, and head circumference by gestational age and sex: the Newborn Cross-

546   Sectional Study of the INTERGROWTH-21st Project., Lancet (London, England).

547   384 (2014) 857–68. https://doi.org/10.1016/S0140-6736(14)60932-6.

548   [26]P.A. Yushkevich, J. Piven, H.C. Hazlett, R.G. Smith, S. Ho, J.C. Gee, G. Gerig,

549   User-guided 3D active contour segmentation of anatomical structures:

550   significantly improved efficiency and reliability., NeuroImage. 31 (2006) 1116–28.

551   https://doi.org/10.1016/j.neuroimage.2006.01.015.

552   [27]K.H. Zou, S.K. Warfield, A. Bharatha, C.M.C. Tempany, M.R. Kaus, S.J. Haker,

553   W.M. Wells, F.A. Jolesz, R. Kikinis, Statistical Validation of Image Segmentation

554   Quality Based on a Spatial Overlap Index, Acad Radiol. 11 (2004) 178–189.

555   https://doi.org/10.1016/S1076-6332(03)00671-8.

556   [28]J. Hutter, L. Jackson, A. Ho, M. Pietsch, L. Story, L.C. Chappell, J. V. Hajnal, M.

557   Rutherford, T2* relaxometry to characterize normal placental development over

558   gestation in-vivo at 3T, Wellcome Open Research. 4 (2019) 166.

559   https://doi.org/10.12688/wellcomeopenres.15451.1.

560   [29]A.R. Backes, A new approach to estimate lacunarity of texture images, Pattern

561   Recognition Letters. 34 (2013) 1455–1461.

562   https://doi.org/10.1016/j.patrec.2013.05.008.

563   [30]F. Pedregosa, G. Varoquaux, A. Gramfort, V. Michel, B. Thirion, O. Grisel, M.

564   Blondel, A. Müller, J. Nothman, G. Louppe, P. Prettenhofer, R. Weiss, V.

565   Dubourg, J. Vanderplas, A. Passos, D. Cournapeau, M. Brucher, M. Perrot, É.

566   Duchesnay, Scikit-learn: Machine Learning in Python, Journal of Machine

567   Learning Research. 12 (2012) 2825–2830.

568   [31]A.F. Marquand, I. Rezek, J. Buitelaar, C.F. Beckmann, Understanding

569   Heterogeneity in Clinical Cohorts Using Normative Models: Beyond Case-Control

570   Studies, Biological Psychiatry. 80 (2016) 552–561.

571   https://doi.org/10.1016/j.biopsych.2015.12.023.

572   [32]I.M. Beune, F.H. Bloomfield, W. Ganzevoort, N.D. Embleton, P.J. Rozance, A.G.

573   van Wassenaer-Leemhuis, K. Wynia, S.J. Gordijn, Consensus Based Definition of

574   Growth Restriction in the Newborn, J Pediatr. 196 (2018) 71-76.e1.

575   https://doi.org/10.1016/j.jpeds.2017.12.059.

576   [33]G. Mielke, N. Benda, Cardiac output and central distribution of blood flow in the

577   human fetus., Circulation. 103 (2001) 1662–8.

578   https://doi.org/10.1161/01.cir.103.12.1662.

579   [34]M. Seed, J. F P van Amerom, S.-J. Yoo, B. Nafisi, L. Grosse-Wortmann, E. Jaeggi,

580   M.S. Jansz, C.K. Macgowan, Feasibility of quantification of the distribution of

581   blood flow in the normal human fetal circulation using CMR: a cross-sectional

582   study, Journal of Cardiovascular Magnetic Resonance. 14 (2012) 79.

583   https://doi.org/10.1186/1532-429X-14-79.

584   [35]N.B. Matthiesen, T.B. Henriksen, P. Agergaard, J.W. Gaynor, C.C. Bach, V.E.

585   Hjortdal, J.R. Østergaard, Congenital Heart Defects and Indices of Placental and

586   Fetal Growth in a Nationwide Study of 924 422 Liveborn Infants, Circulation. 134

587   (2016) 1546–1556. https://doi.org/10.1161/CIRCULATIONAHA.116.021793.

588   [36]E. Llurba, O. Sánchez, Q. Ferrer, K.H. Nicolaides, A. Ruíz, C. Domínguez, J.

589   Sánchez-de-Toledo, B. García-García, G. Soro, S. Arévalo, M. Goya, A. Suy, S.

590   Pérez-Hoyos, J. Alijotas-Reig, E. Carreras, L. Cabero, Maternal and foetal

591   angiogenic imbalance in congenital heart defects, European Heart Journal. 35

592   (2014) 701–707. https://doi.org/10.1093/eurheartj/eht389.

593   [37]C.E.G. Head, V.C. Jowett, G.K. Sharland, J.M. Simpson, Timing of presentation

594   and postnatal outcome of infants suspected of having coarctation of the aorta

595   during fetal life, Heart. 91 (2005) 1070–1074.

596   https://doi.org/10.1136/hrt.2003.033027.

597   [38]J.O. Miranda, L. Hunter, S. Tibby, G. Sharland, O. Miller, J.M. Simpson, Myocardial

598   deformation in fetuses with coarctation of the aorta: a case-control study,

599   Ultrasound Obstet Gynecol. 49 (2017) 623–629.

600   https://doi.org/10.1002/uog.15939.

601   [39] W. You, N.N. Andescavage, K. Kapse, M.T. Donofrio, M. Jacobs, C.

602   Limperopoulos, Hemodynamic Responses of the Placenta and Brain to Maternal

603   Hyperoxia in Fetuses with Congenital Heart Disease by Using Blood Oxygen-

604   Level Dependent MRI., Radiology. (2019) 190751.

605   https://doi.org/10.1148/radiol.2019190751.

606   [40] J. Co-Vu, D. Lopez-Colon, H.V. Vyas, N. Weiner, C. DeGroff, Maternal

607   hyperoxygenation: A potential therapy for congenital heart disease in the fetuses?

608   A systematic review of the current literature, Echocardiography. 34 (2017) 1822–

609   1833. https://doi.org/10.1111/echo.13722.

610   [41] Q.N. Do, M.A. Lewis, A.J. Madhuranthakam, Y. Xi, A.A. Bailey, R.E. Lenkinski,

611   D.M. Twickler, Texture analysis of magnetic resonance images of the human

612   placenta throughout gestation: A feasibility study, PLOS ONE. 14 (2019)

613   e0211060. https://doi.org/10.1371/journal.pone.0211060.

614   [42] N. Andescavage, S. Dahdouh, M. Jacobs, S. Yewale, D. Bulas, S. Iqbal, A.

615   Baschat, C. Limperopoulos, In vivo textural and morphometric analysis of

616   placental development in healthy & growth-restricted pregnancies using magnetic

617   resonance imaging, Pediatric Research. 85 (2019) 974–981.

618   https://doi.org/10.1038/s41390-019-0311-1.

619   [43] A.M. El-Ali, W. Reynolds, V. Rajagopalan, V. Lee, J. Wallace, J. Schabdach, A.

620   Zehner, M. Gruss, J.H. Adibi, V. Schmithorst, A. Panigrahy, BOLD MR Imaging of

621   Placenta in Congenital Heart Disease: Correlation with Maternal Risk Factors,

622   Placental Pathology, and Maternal Serum Hormones [abstract], ISMRM 27th

623   Annual Meeting & Exhibition. (2019). https://doi.org/10.1101/388074.

624   [44] E.A. Turk, S.M. Abulnaga, J. Luo, J.N. Stout, H.A. Feldman, A. Turk, B. Gagoski,

625   L.L. Wald, E. Adalsteinsson, D.J. Roberts, C. Bibbo, J.N. Robinson, P. Golland,

626   P.E. Grant, W.H. Barth, Placental MRI: Effect of maternal position and uterine

627   contractions on placental BOLD MRI measurements, Placenta. (2020).

628   https://doi.org/10.1016/j.placenta.2020.04.008.

629   [45] S.J. Gordijn, I.M. Beune, B. Thilaganathan, A. Papageorghiou, A.A. Baschat, P.N.

630   Baker, R.M. Silver, K. Wynia, W. Ganzevoort, Consensus definition of fetal growth

631   restriction: a Delphi procedure, Ultrasound in Obstetrics & Gynecology. 48 (2016)

632   333–339. https://doi.org/10.1002/uog.15884.

633   [46] N.B. Matthiesen, T.B. Henriksen, J.W. Gaynor, P. Agergaard, C.C. Bach, V.E.

634   Hjortdal, J.R. Østergaard, Congenital Heart Defects and Indices of Fetal Cerebral

635 Growth in a Nationwide Cohort of 924 422 Liveborn Infants., Circulation. 133

636 (2016) 566–75. https://doi.org/10.1161/CIRCULATIONAHA.115.019089.

637 [47]R. Avni, O. Golani, A. Akselrod-Ballin, Y. Cohen, I. Biton, J.R. Garbow, M.

638 Neeman, MR Imaging–derived Oxygen-Hemoglobin Dissociation Curves and

639 Fetal-Placental Oxygen-Hemoglobin Affinities, Radiology. 280 (2016) 68–77.

640 https://doi.org/10.1148/radiol.2015150721.

641 [48]L. Sun, D. Marini, B. Saini, E. Schrauben, C.K. Macgowan, M. Seed,

642 Understanding Fetal Hemodynamics Using Cardiovascular Magnetic Resonance

643 Imaging, FDT. 47 (2020) 354–362. https://doi.org/10.1159/000505091.

644 [49]J. Hutter, A.A. Harteveld, L.H. Jackson, S. Franklin, C. Bos, M.J.P. Osch, J.

645 O'Muircheartaigh, A. Ho, L. Chappell, J. V. Hajnal, M. Rutherford, E. De Vita,

646 Perfusion and apparent oxygenation in the human placenta (PERFOX), Magnetic

647 Resonance in Medicine. 83 (2020) 549–560. https://doi.org/10.1002/mrm.27950.

648 [50]A. Melbourne, R. Aughwane, M. Sokolska, D. Owen, G. Kendall, D. Flouri, A.

649 Bainbridge, D. Atkinson, J. Deprest, T. Vercauteren, A. David, S. Ourselin,

650 Separating fetal and maternal placenta circulations using multiparametric MRI,

651 Magnetic Resonance in Medicine. 81 (2019) 350–361.

652 https://doi.org/10.1002/mrm.27406.

653 [51]N.S. Dellschaft, G. Hutchinson, S. Shah, N.W. Jones, C. Bradley, L. Leach, C.

654 Platt, R. Bowtell, P.A. Gowland, The haemodynamics of the human placenta in

655 utero, PLOS Biology. 18 (2020) e3000676.

656 https://doi.org/10.1371/journal.pbio.3000676.

657 [52]P.J. Slator, J. Hutter, L. McCabe, A.D.S. Gomes, A.N. Price, E. Panagiotaki, M.A.

658 Rutherford, J.V. Hajnal, D.C. Alexander, Placenta microstructure and

659 microcirculation imaging with diffusion MRI, Magnetic Resonance in Medicine. 80

660 (2018) 756–766. https://doi.org/10.1002/mrm.27036.

661 [53]Z. Zun, G. Zaharchuk, N.N. Andescavage, M.T. Donofrio, C. Limperopoulos, Non-

662 Invasive Placental Perfusion Imaging in Pregnancies Complicated by Fetal Heart

663 Disease Using Velocity-Selective Arterial Spin Labeled MRI., Scientific Reports. 7

664 (2017) 16126. https://doi.org/10.1038/s41598-017-16461-8.

665 [54]Z. Zun, C. Limperopoulos, Placental perfusion imaging using velocity-selective

666 arterial spin labeling, Magn Reson Med. 80 (2018) 1036–1047.

667 https://doi.org/10.1002/mrm.27100.

668

Tables/figures

|	Median	IQR	Min	Max	p
Control cohort (n=37)					
Maternal age at scan (a)	34.65	4.65	27.69	44.03	
Maternal BMI at scan (kg/m^2)	30.03	8.67	18.75	42.59	
Gestational age at scan (w)	30.86	8.36	19.57	37.86	
Fetal sex (female/total)	0.62				
Gestational age at birth (w)	40.14	2.14	38.14	42.14	
Birth weight (g)	3583	534	2780	4450	
BW Z-score	0.9558	1.2147	-1.0550	2.1966	
BW Centile	83.04	39.16	14.57	98.60	
CHD cohort (n=69)					
Maternal age at scan (a)	32.63	8.39	18.60	40.79	0.002†
Maternal BMI at scan (kg/m^2)	28.39	5.63	18.81	40.35	0.094†
Gestational age at scan (w)	31.57	2.64	28.43	36.29	0.069†
Fetal sex (female/total)	0.58				0.836
Gestational age at birth (w)	38.71	1.57	32.71	41.71	<0.001
Birth weight (g)	3080	964	1610	5150	<0.001
BW Z-score	-0.1230	1.7762	-2.9547	3.7986	0.003
BW Centile	48.20	62.20	0.16	99.99	0.003
Diagnosis	N	%			
Left-sided obstructive lesions	10	14.5	HLHS		
	13	18.8	COA- (suspected, not confirmed)		
	8	11.6	COA+ (confirmed neonatal)		
Right-sided obstructive lesions	10	14.5	TOF, PA, PS, TA, Ebstein anomaly		
Disorders of mixing	5	7.2	TGA		
Suspected vascular rings	17	24.6	DAA, RAA (+/- ALSA)		
Other major lesions	6	8.7	CAT, PAPVD, CR		

Table 1: Maternal and pregnancy characteristics.

(†) For statistical analysis controls were restrained to GA range at scan (28 – 37 weeks, N=23).

Mean deviation from GP [Z-score] +/- SD of Z-scores within group									
	Control	CHD	HLHS	COA-	COA+	RSOL	TGA	Other	VR
N	9	69	10	13	8	10	5	6	17
Mean T2*	-0.56 +/-1.34	0.93* +/-2.26	0.64 +/-2.03	1.39* +/-2.91	0.24 +/-1.34	2.30*** +/-2.07	-0.11 +/-1.86	2.31** +/-2.01	0.09 +/-2.06
Skewness	-0.08 +/-0.59	-1.99* +/-4.27	-1.12 +/-1.58	-3.83 +/-7.18	-0.66 +/-0.73	-4.69* +/-5.56	0.02 +/-0.73	-1.75** +/-1.25	-0.80 +/-2.70
Kurtosis	-0.53 +/-1.01	-1.67 +/-2.34	-0.98 +/-1.39	-2.86* +/-3.25	-0.98 +/-0.67	-3.47** +/-3.02	-0.27 +/-1.50	-1.97** +/-0.93	-0.73 +/-1.66
Lacunarity	-0.15 +/-1.27	-0.54 +/-1.55	-0.18 +/-1.21	-1.02 +/-1.69	0.26 +/-0.53	-1.70* +/-1.99	-0.01 +/-0.98	-1.26 +/-2.35	0.06 +/-0.93
Median deviation from GP [Z-score] (IQR within group)									
	Control	CHD	HLHS	COA-	COA+	RSOL	TGA	Other	VR
N	9	69	10	13	8	10	5	6	17
Mean T2*	-0.78 (2.05)	0.70* (2.93)	0.57 (2.37)	0.89* (4.05)	0.25 (2.06)	2.36*** (3.32)	-0.41 (3.68)	2.10** (3.77)	-0.59 (2.76)
Skewness	0.01 (0.71)	-0.47* (2.19)	-0.49 (2.94)	-0.96 (4.38)	-0.62 (0.98)	-2.12* (10.23)	0.73 (2.32)	-1.89** (2.40)	0.02 (0.83)
Kurtosis	-0.80 (1.67)	-1.10 (1.95)	-0.75 (2.07)	-1.72* (3.35)	-0.86 (1.04)	-2.15** (5.64)	0.41 (2.65)	-1.83** (1.83)	-0.63 (1.23)
Lacunarity	0.01 (1.95)	-0.18 (1.67)	-0.09 (1.28)	-0.68 (2.49)	0.17 (0.82)	-1.43* (2.22)	0.29 (1.84)	-0.37 (3.84)	0.05 (1.35)

673 **Table 2: Results Gaussian process Regression, groupwise.**

674 Entire CHD cohort (CHD), Hypoplastic left heart syndrome (HLHS), Coarctation

675 suspected not confirmed (CoA-), Coarctation confirmed operated (CoA+), Right-sided

676 obstructive lesions (RSOL), Disorders of mixing (TGA), Other lesions, Suspected

677 vascular rings (VR). Significance calculated by Independent t-test (Mean T2*) or Mann-

678 Whitney U (Skewness, Kurtosis, Lacunarity) in comparison to test control cohort, *

679 $p \leq 0.05$, ** $p \leq 0.01$, *** $p \leq 0.001$.

680
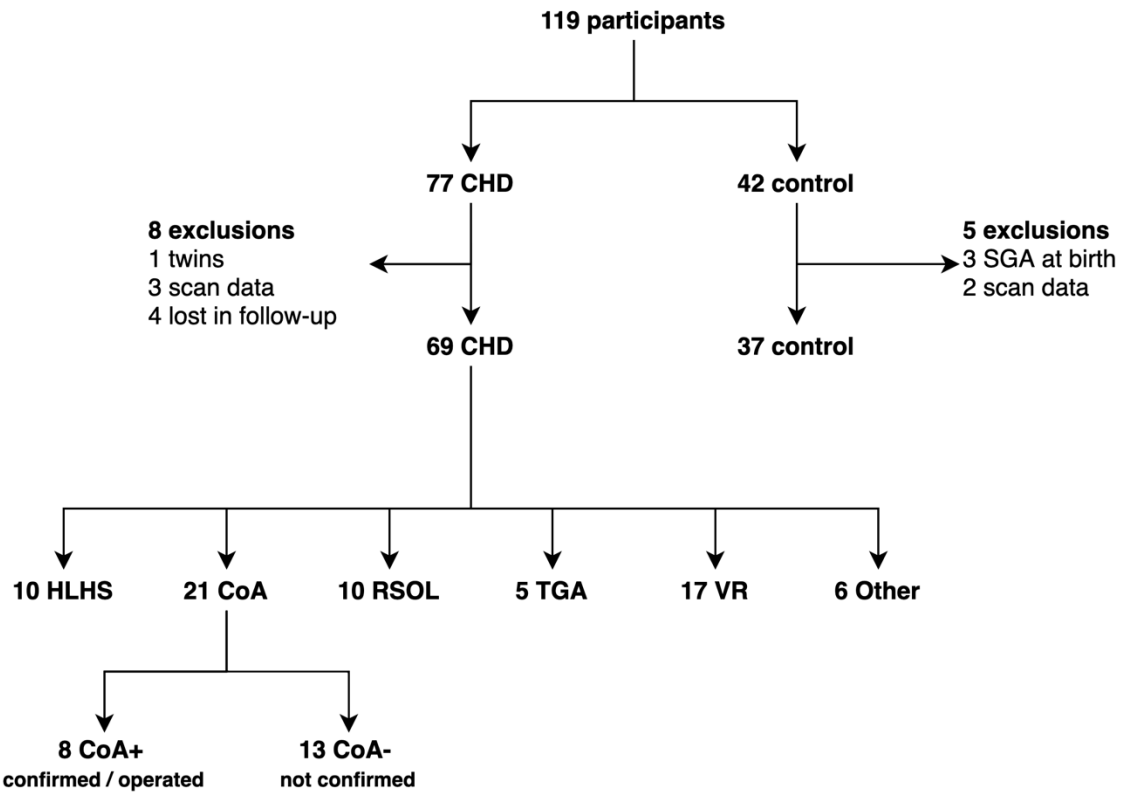
Figure 1 - Study cohort.

CHD subtypes classified by main antenatal diagnosis: Hypoplastic left heart (HLHS),
coarctation of the aorta (CoA), right-sided obstructive lesions (RSOL), transposition of
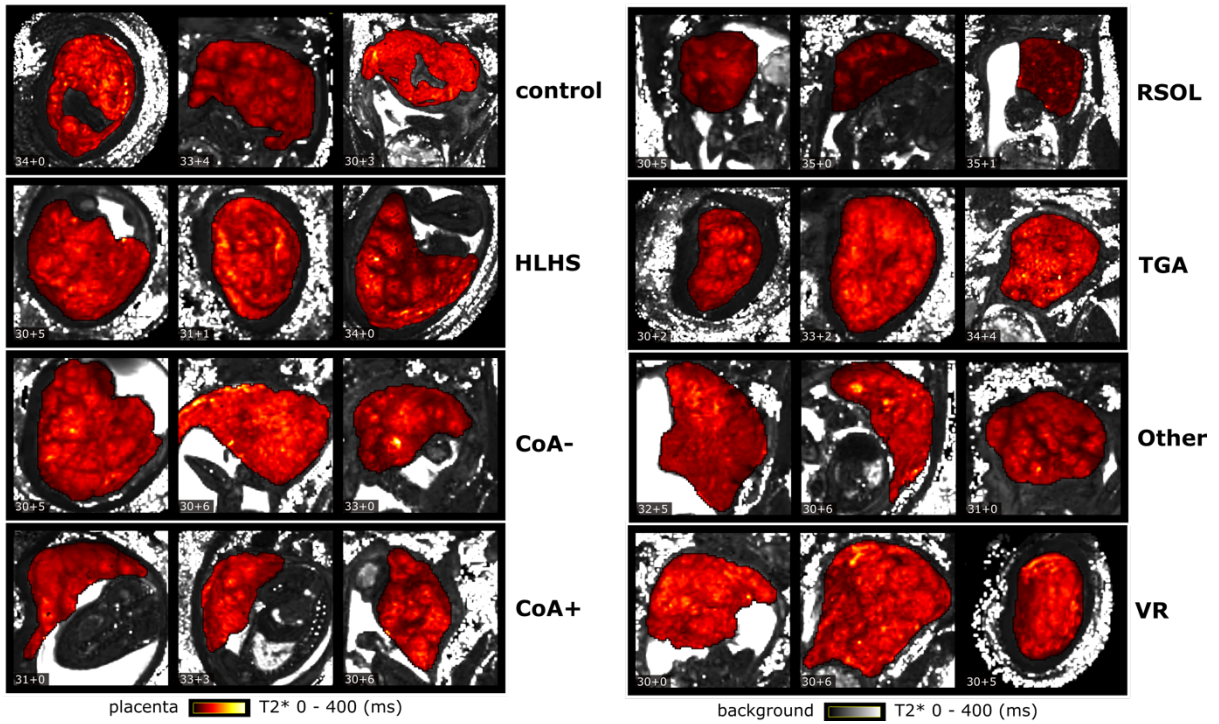the great arteries (TGA), suspected vascular ring (VR) and other complex lesions.
Controls were excluded for low birth weight (SGA) and insufficient scan data,
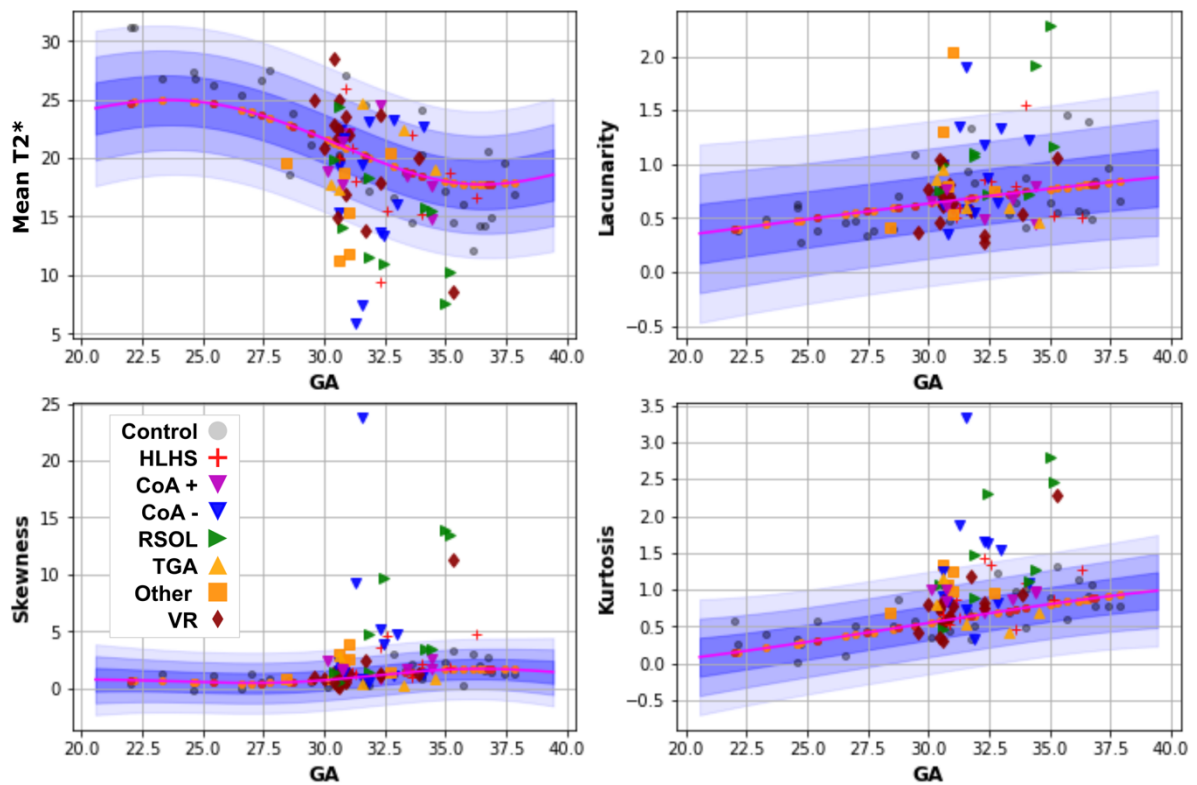pregnancies complicated by fetal CHD had to be excluded for twin pregnancy and loss
in follow-up at time of analysis.

688

Figure 2: Qualitative Imaging

Illustration of mid-stack slice in coronal orientation from T2* maps from 3 individual placentas for all included cohorts. Segmented placental parenchyma is highlighted in red/yellow scales.

Figure 3 – Gaussian Process Regression results

The posterior probability for Mean T2*, Lacunarity, Skewness and Kurtosis over GA for all considered controls in red, the corridors corresponding to Z-scores of 1, 2 and 3 are illustrated in blue. Cohorts: Control (test subset), Hypoplastic left heart syndrome (HLHS), Coarctation of the aorta confirmed (COA+) and not confirmed (COA-), right-sided obstructive lesions (RSOL), disorders of mixing (TGA), other major lesions and suspected vascular rings (VR).

702
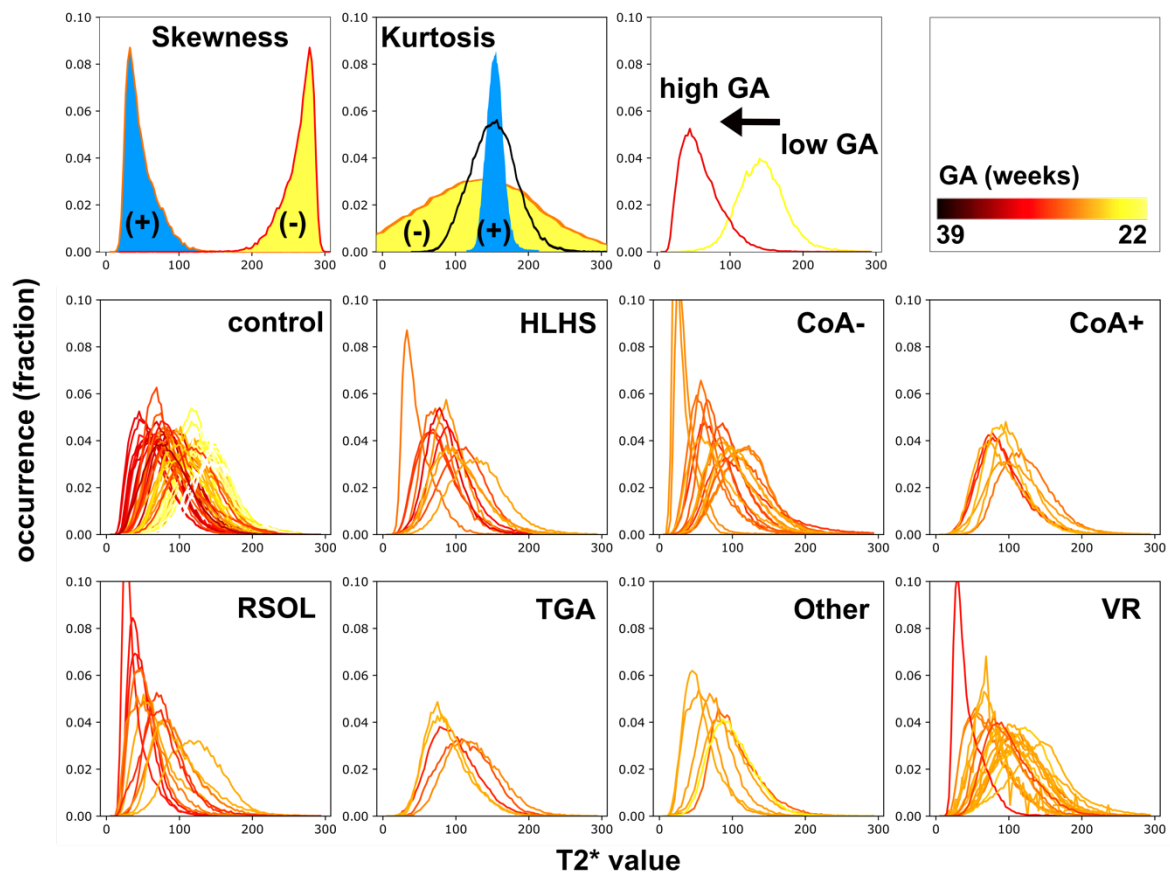
Figure 4 - Individual Histograms

Individual Histograms, derived from about 70000 voxels per subject binned in 100,
depicting occurrence fraction of T2* values over the entire placental volume from all
participants, coloured by GA at scan. Groups from top left to bottom right. Control,
Hypoplastic left heart syndrome (HLHS), coarctation of the aorta not confirmed (CoA-)
and confirmed (COA+), right-sided obstructive lesion (RSOL), Transposition of the
great arteries (TGA), Other lesions and suspected vascular ring (VR).
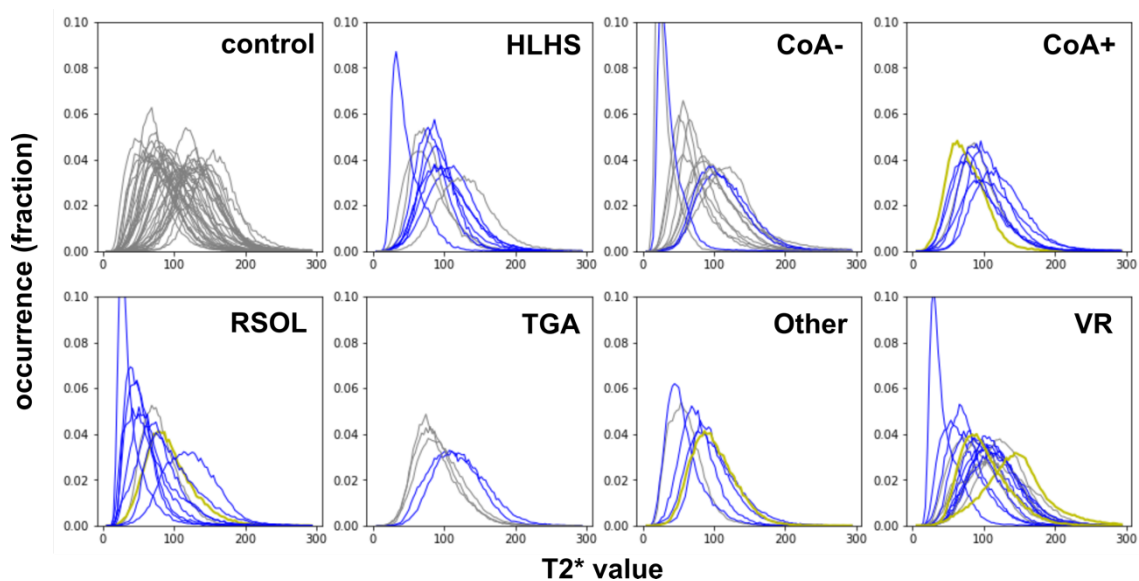
Supplemental Figure 1 – Histograms with genetic test results

Individual Histograms, as shown in Figure 4. Color coded by results of genetic testing. Abnormal genetics (yellow), normal genetics (blue), not tested (grey), Hypoplastic left heart syndrome (HLHS), coarctation of the aorta not confirmed (CoA-) and confirmed (COA+), right-sided obstructive lesion (RSOL), Transposition of the great arteries (TGA), Other lesions and suspected vascular ring (VR).
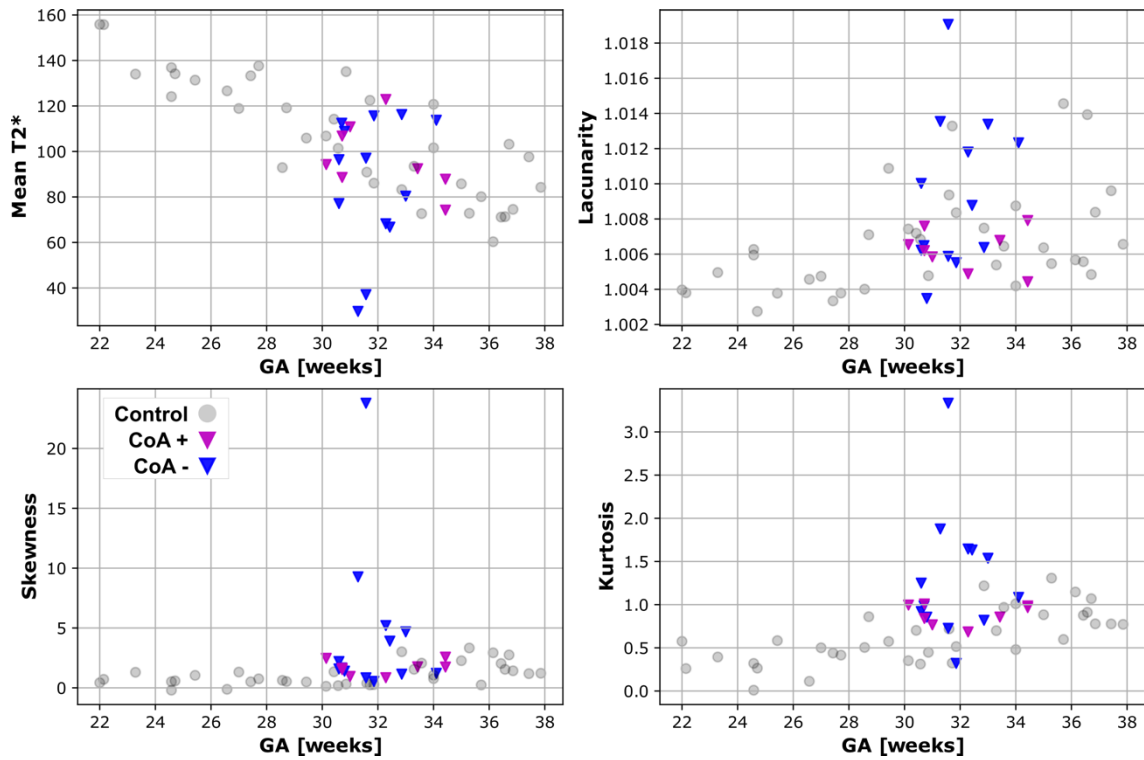
N (%)	Control	CHD
Available placental histology	15/37 (40%)	12/69 (17%)
MVM	1	2
With infarct	1	2
(Sub-)Chorionitis	8	7
With MIR	4	3
With FIR	5	4

Supplemental Table 1 – Placental Histology

Table shows available placental histology results. Maternal vascular malperfusion (MVM), maternal inflammatory response (MIR), fetal inflammatory response (FIR).

Supplemental Figure 2 – Coarctation of the aorta cohort and controls

Mean T2*, Lacunarity, Skewness and Kurtosis over GA for all included controls in grey, confirmed Coarctation of the aorta (CoA+) in pink and not confirmed (CoA-) in blue.